Longitudinal to Transverse Metachronal Wave Transitions in an *In Vitro* Model of Ciliated Bronchial Epithelium

Olivier Mesdjian,[1] Chenglei Wang,[2,3,*] Simon Gsell,[2] Umberto D'Ortona,[2] Julien Favier,[2] Annie Viallat,[1] and Etienne Loiseau[1,†]

[1]*Aix Marseille University, CNRS, CINAM, Turing Centre for Living Systems, 13009 Marseille, France*
[2]*Aix Marseille University, CNRS, Centrale Marseille M2P2, France*
[3]*Department of Mechanical Engineering, The Hong Kong Polytechnic University, Kowloon, Hong Kong SAR, China*

(Received 6 October 2021; accepted 22 June 2022; published 15 July 2022)

Myriads of cilia beat on ciliated epithelia, which are ubiquitous in life. When ciliary beats are synchronized, metachronal waves emerge, whose direction of propagation depends on the living system in an unexplained way. We show on a reconstructed human bronchial epithelium *in vitro* that the direction of propagation is determined by the ability of mucus to be transported at the epithelial surface. Numerical simulations show that longitudinal waves maximize the transport of mucus while transverse waves, observed when the mucus is rigid and still, minimize the energy dissipated by the cilia.

DOI: 10.1103/PhysRevLett.129.038101

From swimming microorganisms to major organs, multiciliated cells are ubiquitous in living systems. Active cilia support multiple biological functions such as the motility and feeding of marine microorganisms, circulation of the cerebrospinal fluid in the central nervous system, and mucociliary clearance of pathogens and pollutants from airways [1,2]. The generation of fluid flows at the scale of a microorganism or at the tissue level requires a dense array of cilia that coordinate both their beat directions [3,4] and their phase [5]. Such coordination results from hydrodynamic coupling between cilia [6]. When neighboring cilia maintain a constant phase difference, metachronal waves emerge [7].

Physical models have been developed to address the conditions of wave emergence and their possible advantage for biological systems [8–13]. Guirao and Joanny [14] proposed that metachronal coordination arises from self-organization and hydrodynamic coupling that improves the steadiness of the resulting flow. Numerical simulations have solved the fluid-structure interaction of flexible cilia beating in fluid [15,16]. They found that metachrony results in an increased-velocity transport and efficiency. Elgeti *et al.* [15] predicted the emergence of waves propagating in various directions: longitudinal, transverse, and oblique. Yet, the role of the direction of propagation is not clear.

Experimentaly, cilia arrays on the surface of swimming and marine microorganisms exhibit metachronal waves propagating in different directions [17,18], but the majority present transverse waves. On the contrary, observations made *ex vivo* on animal bronchial epithelia report the presence of longitudinal waves [19–21]. These experimental results suggest that the direction of propagation may play a role to optimize a given biological function. The relationships between the type of metachronism, the biophysical parameters the living system optimizes, and the physiological function are still unclear. Indeed, nonequilibrium active systems are frustrated systems that cannot simultaneously solve all energy minimization associated with each biological, physical, and physiological constraint. As a consequence, the whole phase space of the parameters is not accessible to the biological system. An experimental system where the emergence of metachrony can be tuned would be a major asset to decipher such relationships.

Here, we experimentally manage to control the direction of metachronal waves that emerge at the surface of an *in vitro* reconstituted bronchial epithelium by tuning the boundary conditions on top of cilia. We show that longitudinal waves propagate when mucus is transported at the epithelial surface, while the presence of a stuck layer of mucus above cilia results in a transition towards transverse waves. We develop a computational model for which we impose the two experimental conditions at the top of the cilia: slip (fluid transport) or no-slip (immobile fluid). We show that longitudinal waves are better suited to transport fluid (higher flux) in slip conditions, while in no-slip conditions, transverse waves minimize the power dissipated by cilia unable to propel mucus.

Experimental system.—The bronchial epithelium is reconstituted *in vitro* at the air-liquid interface and is composed of basal cells, goblet cells that produce mucus, and ciliated cells. The latter cover 80% of the epithelial surface. The apical surface of a ciliated cell (about 30 μm^2) bears as many as 200–300 beating cilia [22] of 7 μm height and gathered into 10–20 bundles (see Movie 1 in the Supplemental Material [23]). Cilia beat in an aqueous periciliary layer of low viscosity [32] and propel a layer of mucus at their tips along the epithelial surface [Fig. 1(a)].

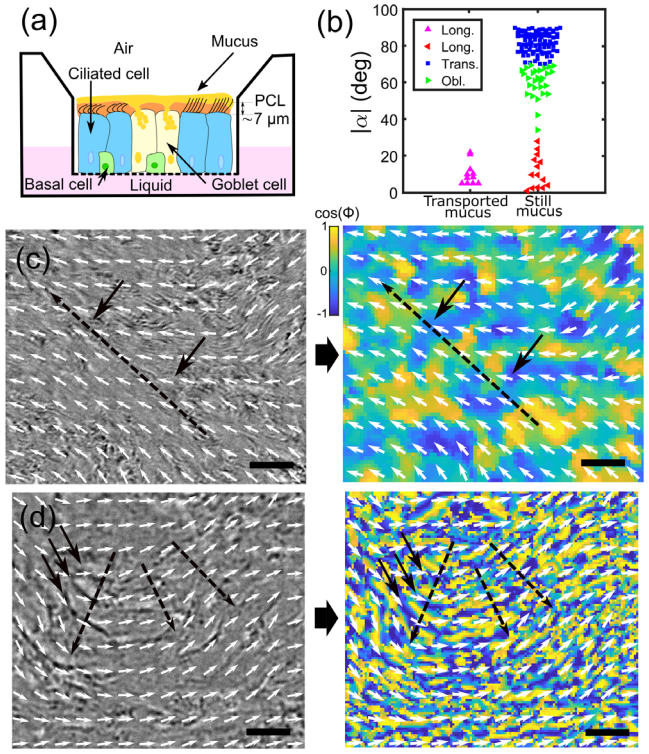

FIG. 1. (a) Schematic of an air-liquid culture of a reconstituted human bronchial epithelium. Cilia beat in the aqueous periciliary layer, and their tips poke in the above mucus layer during the forward stroke. (b) Angle $|\alpha|$ between the direction of propagation of the metachronal wave and the ciliary beat direction in transported and still mucus conditions. (c),(d) Longitudinal wave and transverse wave in the transported and still mucus conditions, respectively. The panels on the left display bright-field images of the propagating waves. The direction of propagation is indicated by the dotted arrow, and the wave fronts are indicated by black solid arrows. The panels on the right show the corresponding map of $\cos(\Phi)$, with Φ being the local phase of the beat pattern (see Fig. 1 in the Supplemental Material for details [23]). The white arrows indicate the local power stroke direction of the cilia. Scale bar = 20 μm.

Materials and methods.—Cultures of human bronchial epithelium reconstituted from primary cells in 6 mm diameter transwells were purchased from Epithelix (MucilAir). The cultures were maintained in an incubator at 37 °C and 5% CO_2. The Epithelix MucilAir culture medium (700 μL) was replaced every 2 days. The mucus on the apical epithelial surface was either kept moist by adding 3 μL of culture medium to the surface once a week to compensate for evaporation processes, which was sufficient to maintain a rotating transport of mucus on the epithelial surface (see Movie 2 in the Supplemental Material [23] and Refs. [3,4]), or allowed to dry spontaneously to gradually form a "crust" of mucus. In the latter case, mucus transport speed gradually decreased until only short-range vibrations were observed (Movie 3 [23]), but the beating of the cilia under the mucus layer could still be observed. In total, we worked on four wells with moistened mucus from three donors, and five wells with dried mucus from three donors.

Cultures were observed in bright field on a Nikon Eclipse Ti inverted microscope with a 20× objective and 1.5× magnification lens, at 37 °C under humidified airflow with 5% CO_2 with a Photron camera (Fastcam, mini-UX50) at 250 fps or a Luminera camera (Infinity 3 Luminera USB) at 40 fps. We performed a gentle apical washing before imaging by adding and removing 200 μL of culture medium.

Emergence of metachronal waves at the epithelial surface.—At the scale of a ciliated cell, we observe bundles of cilia that beat at a frequency ranging between 7 and 12 Hz (see Fig. 2 in the Supplemental Material [23]). On a single cell, we observe that the bundles have the same frequency and the same beating direction. Bundles aligned along the beating direction beat synchronously over a typical length scale of a ciliated cell (~5–6 μm). In the direction perpendicular to the beating direction, phase shifts between the beats of the different bundles are observed, which become significant at the scale of half a cell (see Movie 1 in the Supplemental Material [23]). Indeed, the distance between neighboring bundles on the apical surface of the same cell being less than the length of a cilia, steric constraints impose synchronization along the stroke direction.

At the tissue scale, we observe the propagation of localized metachronal waves on the epithelial surface. We quantify the distance of propagation of the waves from kymographs that are plotted along the direction of propagation (see Fig. 3 in the Supplemental Material). The typical distance of propagation is of the order of 40 μm—i.e., over approximately eight cells—and the width of the wavefront ranges from 20 to 40 μm [see Figs. 1(c) and 1(d)]. The metachronal waves are observed regardless of the collective direction of the ciliary beats, whether linear or circular (see Movie 6 in the Supplemental Material [23]).

We observe three different types of metachronal waves characterized by the angle α between the direction of propagation and the ciliary beating direction [see Fig. 1(b)]. The first type gathers longitudinal waves ($|\alpha| < 15°$), which propagate in the same direction as the forward stroke (symplectic waves). Interestingly, this type of metachrony is the only one that emerges on cultures where the mucus is continuously transported [see Figs. 1(b) and 1(c), and Movies 4–5 in the Supplemental Material [23]]. On rare occasions, symplectic waves emerge on cultures with dried and still mucus [Fig. 1(b)]. The two other types of metachronal waves are observed exclusively on cultures with dried still mucus: (i) transverse waves which propagate perpendicularly to the direction of the ciliary beats [Figs. 1(c) and 1(b), and Movies 6–8 [23]], and (ii) oblique waves that propagate along a direction that makes an angle $|\alpha|$ between 30° and 70° with regard to the beating direction

[Fig. 1(b) and Movie 9 [23]]. Transverse and oblique waves are either laeoplectic or dexioplectic—i.e., they propagate towards the right and the left with respect to the forward stroke. These two types of metachrony emerge with an equal probability. Interestingly, both laeoplectic and dexioplectic waves are observed simultaneously on a given sample.

We measure the wavelength and the distance of wave propagation on each culture. The distributions are displayed in Fig. 2. The average wavelength of longitudinal waves is 40 μm—i.e., eight cells long. Transverse and oblique waves exhibit the same much shorter wavelength, $\lambda_w = 13$ μm—only about two ciliated cells long [Fig. 2(a)]. The distance of propagation is of the same order of magnitude for the three types of wave, in the range of 15–60 μm [Fig. 2(b)]. It is worth noting that for a wave to be able to propagate, all cilia must beat at the same frequency. We establish frequency maps and identify domains with equal beat frequencies [see Fig. 2(c)], whose size limits the distance of wave propagation. We find that the size of these domains is in the range of 15–60 μm [see Fig. 2(d)], which corresponds well to the propagation distance of the metachronal waves. Note that the same size distribution has been established in the dried mucus condition (see Fig. 4 in the Supplemental Material [23]).

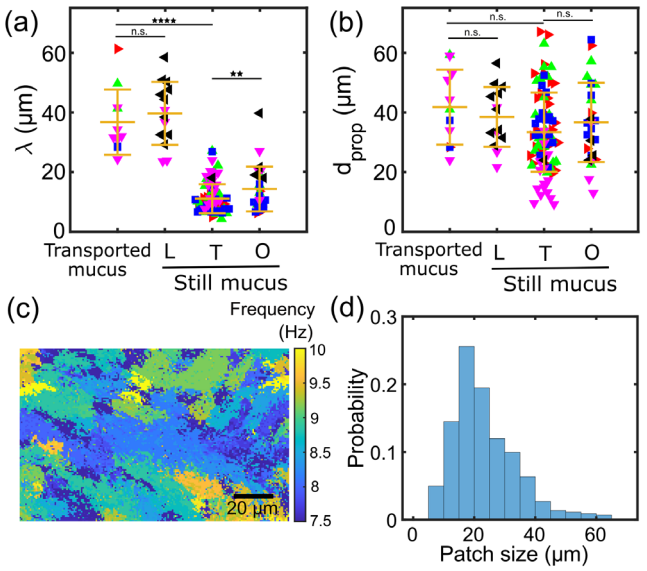

FIG. 2. (a) Distributions of wavelengths λ_w and (b) distance of propagation for longitudinal (L), transverse (T), and oblique (O) waves in transported mucus and still mucus conditions. Each color represents a different culture: $N = 4$ cultures in the transported mucus condition, and $N = 5$ cultures in the still mucus condition. The yellow horizontal bars indicate averages ± 1 standard deviation. $^{**}p < 0.01$; $^{****}p < 0.0001$; n.s.: not significant. (c) Map of ciliary beat frequencies computed with FFT analysis (see Fig. 1 in the Supplemental Material for details [23]) in the transported mucus condition. (d) Size distribution of isofrequency patches. The total area selected for the measurements is 420 μm $\times$ 340 μm.

To understand the mechanisms at the origin of the emergence of the different observed metachronal waves, we have developed a numerical hydrodynamic model of flexible cilia.

The model.—We modeled a cilium as a slender elastic body of diameter D and length L, with $D \ll L$. Within a certain wave of wavelength λ, N cilia are aligned with interciliary distance $\Delta = \lambda/N$, and they are forced to beat in a wavelike form in space and time. To achieve a continuous beat and tunable duration of power and recovery strokes, the internal actuation of the ith cilium is set by its basal angle, which can be written as

$$\theta_i = \Theta \cos(\omega t + \phi_i), \tag{1}$$

where Θ is the angular amplitude, ω is the nominal angular frequency varying from the power to recovery stroke, ϕ_i is the temporal- and spatial-dependent phase angle [see Eq. (4) in the Supplemental Material for details [23]], and $i = 1, 2, 3, \ldots N$. The cilium dynamics is governed by the equation of elasticity described in Ref. [33], with a time-dependent bending rigidity. We obtained a two-dimensional beating pattern characterized by a fast power stroke with an elongated shape and a slow recovery stroke with a bent shape. This pattern is in good agreement with those described in the literature [19] [see Fig. 3(a)]. The forward stroke is in the increasing x direction. The dynamics of the three-dimensional incompressible flow, described by the continuity and momentum equations, is solved using the lattice Boltzmann method, following Ref. [16]. The fluid is considered as Newtonian with a Reynolds number fixed to 0.1. To account for the unsteady flexible boundaries, we use the immersed boundary method (IBM), following the numerical framework proposed in Ref. [33] (see details about the simulation method in the Supplemental Material [23]). Cilia are placed along a line in the numerical domain at a spacing of $\Delta = 0.5L$ or $\Delta = 1L$ depending on the boundary conditions. The transverse waves are obtained by setting the cilia along the y axis [see Fig. 3(b)], whereas the longitudinal waves are obtained by setting the cilia along the x axis [see Fig. 3(c)]. The height of the domain h is fixed to $1.2L$. On top of the cilia, we modeled the flowing mucus condition or the dried still mucus condition with either a slip or no-slip condition for the fluid. The wavelength λ is fixed by the number of cilia present in the domain, and the periodic condition is imposed on both the x and y directions. We computed several quantities related to the cilia and the flow.

The nondimensional, time-dependent force and power that one cilium exerts on the fluid are defined as $\vec{F}^*(t) = \int_0^L -\vec{F}_f ds$ and $P^*(t) = \int_0^L \vec{F}_f . \vec{v}_c ds$, respectively, with $\vec{F}_f$ being the force that the fluid exerts on the cilium, and $\vec{v}_c$ the velocity of the cilium. We convert $\vec{F}^*$ and P^* into their respective dimensional quantities $\vec{F} = \vec{F}^* \times (EI/L^2)$ and $P = P^* \times (V_c EI/L^2)$, where EI is the bending rigidity of

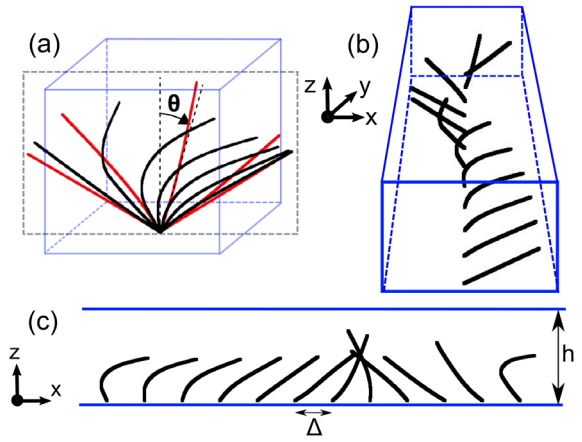

FIG. 3. (a) Beat pattern of a cilium of length L. The positions of the cilium during the fast-forward stroke are represented in red, while the positions during the slow recovery are in black. The internal actuation of the cilium is set by its basal angle θ. The cilium motion stays in the $y = 0$ plane (black dotted rectangle), with the power stroke oriented towards the increasing x direction. (b) Cilia aligned in the y direction: example of a transverse configuration with $\lambda = 12L$ and $\Delta = 1L$. (c) Cilia aligned in the x direction: example of a longitudinal configuration with $\lambda = 12L$ and $\Delta = 0.5L$. The height of the domain is fixed to $h = 1.2L$.

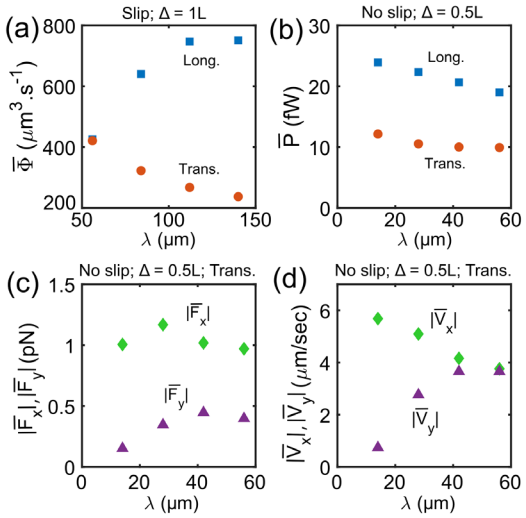

FIG. 4. Averaged quantities numerically computed and plotted as a function of λ. (a) Total mean flux for longitudinal (blue squares) and transverse (red circles) waves in the slip condition with $\Delta = 1L$. (b) Mechanical power dissipated by one cilium for longitudinal (blue squares) and transverse (red circles) waves in the no-slip condition with $\Delta = 0.5L$. In the case of transverse waves, in no-slip condition and $\Delta = 0.5L$, (c) force exerted by a cilium along x (green diamonds) and along y (purple triangles), and (d) local fluid velocity at a cilium position, both along x (green diamonds) and along y (purple triangles). Quantities plotted for an extended range of λ are shown in Fig. 7 of the Supplemental Material [23].

one cilium, L the length of one cilium, and $V_c = 2L/T_b$ the characteristic velocity of one cilium, with $T_b = T_r + T_p$ as the beating period. We use the experimental values found in the literature: $EI = 6 \times 10^{-22}$ N m^2 [34], $L = 7$ μm, and $T = 1/10$ s [19].

As shown in Fig. 5 of the Supplemental Material [23], $P(t)$ exhibits periodically two regions: a first long duration with a small peak corresponding to the cilium recovery stroke beating, and a second shorter duration with a higher peak corresponding to the cilium power stroke beating. We denote $\bar{P}$ (and $\bar{F}$) as the average of $P(t)$ [$F(t)$] on one beating period at steady state.

We also compute the time-dependent flux generated by one cilium in the x direction (or the y direction) crossing the yz plane (the xz plane): $\Phi_x^*(t)$ and $\Phi_y^*(t)$, whose relations with the dimensional flux are $\Phi_x = \Phi_x^* \times (L^3/T_b)$ and $\Phi_y = \Phi_y^* \times (L^3/T_b)$, respectively. These fluxes typically reach a steady state after the first half-period of cilia beating (see Fig. 5 in the Supplemental Material [23]). We deduce the total mean flux generated by one cilium as $\bar{\Phi} = (\bar{\Phi}_x{}^2 + \bar{\Phi}_y{}^2)^{1/2}$, with $\bar{\Phi}_x$ ($\bar{\Phi}_y$) the time average of Φ_x (Φ_y) over one period at steady state.

Finally, we define the mean fluid velocities as $\overline{V_x} = \bar{\Phi}_x/S$ and $\overline{V_y} = \bar{\Phi}_y/S$, where S is the lateral section of the domain corresponding to one cilium, $S = h \times \Delta = (1.2L) \times \Delta$, with $\Delta = 0.5L$ or $\Delta = 1L$.

Slip condition: Efficiency of longitudinal metachronal waves.—Experimental observations show that only longitudinal waves propagate. In the model, we set $\Delta = 1L$, since the length of one cell is approximately the same as one cilium, and at the scale of one multiciliated cell, cilia beat synchronously. We chose to compute the mucus flux based on the reasonable hypothesis that bundles of cilia synchronize themselves in order to maximize mucus transport. Figure 4(a) shows the variation of the flux with the wavelength for both longitudinal and transverse waves. The flux created by the longitudinal waves becomes higher than the flux of the transverse waves for wavelengths larger than ~50 μm, in the range of the observed longitudinal wavelength [Fig. 2(a)]. In principle, we should expect that waves of higher wavelength should be observed since the flux increases with the wavelength. However, the biological system prevents the emergence of such waves due to the limited size (50 μm) of multiciliated cell domains with equal frequency.

No-slip condition: Power dissipation and transverse flow.—Experimental observations show the emergence of transverse waves in the absence of mucus transport. In this condition, as phase shifts are observed at the scale of half a cell, we set $\Delta = 0.5L$ in the model. As the flux is no longer a relevant quantity, we hypothesize that bundles synchronize themselves to minimize the dissipated mechanical power. Figure 4(b) shows the variation of the dissipated power with the wavelength. At all wavelengths, the $\bar{P}$ of transverse waves is about 2 times lower than that of longitudinal waves. This explains the observed emergence

of transverse waves in the absence of mucus transport. However, there is no strong variation of $\bar{P}$ with λ for transverse waves, which could explain why short wavelengths are experimentally observed. In order to have a deeper insight in the system, we have computed the hydrodynamic force and the fluid velocity in the PCL exerted by a cilium. The x and y components of these quantities are shown in Figs. 4(c) and 4(d), respectively. Strikingly, the y component of $\bar{F}$ increases by a factor of 3, and that of $\bar{V}$ by a factor of 8, between $\lambda = 14$ μm and $\lambda = 42$ μm. The x component of $\bar{V}$ decreases from 6 to 4 μm/ sec between $\lambda = 14$ μm and $\lambda = 42$ μm so that at $\lambda = 42$ μm, $|\bar{V}_x| = |\bar{V}_y|$. At all λ values, $\bar{V}$ is of the same order of magnitude, but its direction is progressively shifted from a longitudinal direction for $\lambda = 14$ μm towards 45° for $\lambda = 42$ μm. The flow can be moved even more in the transverse direction if the cilia are set closer than $\Delta = 0.5L$, as shown in Fig. 6 in the Supplemental Material [23]. We consider that such a configuration is unlikely to emerge and remains stable. Indeed, cilia are mechanosensitive organelles which can actively modify their beat directions in response to an external hydrodynamic cue [3,35,36]. Based on these considerations, the numerical model suggests that the system favors the emergence of transverse waves with short wavelengths to prevent a possible destabilization of ciliary beat directions. This corresponds to the previously described experimental observations.

Concluding remarks.—We experimentally showed that the type of metachronism can be modified on the same system and depends on the external conditions. The combination of experimental and numerical approaches suggests that the system optimizes the flux to transport the mucus, while it lowers the energy consumption and prevents any hydrodynamic destabilization of the cilia in the absence of transport. This approach conducted on a major biological system shows that each type of metachronism could be associated with the optimization of a physical quantity, linked with a physiological function or regulation of the biological system. Our study may shed new light on metachronisms in other living systems such as marine organisms.

We thank Dr. K. Khelloufi for providing a movie. The project leading to this publication has received funding from the "Investissements d'Avenir" French government program managed by the French National Research Agency (No. ANR-16-CONV-0001) and from the Excellence Initiative of Aix-Marseille University—A*MIDEX. The Centre de Calcul Intensif d'Aix-Marseille University is acknowledged for granting access to its high-performance computing resources.

*chenglei.wang@polyu.edu.hk
†etienne.loiseau@univ-amu.fr

[1] C. Boutin and L. Kodjabachian, Curr. Opin. Genet. Dev. **56**, 1 (2019).
[2] E. R. Brooks and J. B. Wallingford, Curr. Biol. **24**, R973 (2014).
[3] E. Loiseau, S. Gsell, A. Nommick, C. Jomard, D. Gras, P. Chanez, U. D'Ortona, L. Kodjabachian, J. Favier, and A. Viallat, Nat. Phys. **16**, 1158 (2020).
[4] M.-K. Khelloufi, E. Loiseau, M. Jaeger, N. Molinari, P. Chanez, D. Gras, and A. Viallat, Sci. Rep. **8**, 2447 (2018).
[5] W. Gilpin, M. S. Bull, and M. Prakash, Nat. Rev. Phys. **2**, 74 (2020).
[6] D. R. Brumley, K. Y. Wan, M. Polin, and R. E. Goldstein, eLife **3**, e02750 (2014).
[7] D. R. Brumley, M. Polin, T. J. Pedley, and R. E. Goldstein, J. R. Soc. Interface **12**, 20141358 (2015).
[8] N. Uchida and R. Golestanian, Phys. Rev. Lett. **104**, 178103 (2010).
[9] J. Han and C. S. Peskin, Proc. Natl. Acad. Sci. U.S.A. **115**, 4417 (2018).
[10] S. Gueron and K. Levit-Gurevich, Proc. Natl. Acad. Sci. U.S.A. **96**, 12240 (1999).
[11] A. Takamatsu, K. Shinohara, T. Ishikawa, and H. Hamada, Phys. Rev. Lett. **110**, 248107 (2013).
[12] N. Osterman and A. Vilfan, Proc. Natl. Acad. Sci. U.S.A. **108**, 15727 (2011).
[13] F. Meng, R. R. Bennett, N. Uchida, and R. Golestanian, Proc. Natl. Acad. Sci. U.S.A. **118** (2021).
[14] B. Guirao and J.-F. Joanny, Biophys. J. **92**, 1900 (2007).
[15] J. Elgeti and G. Gompper, Proc. Natl. Acad. Sci. U.S.A. **110**, 4470 (2013).
[16] S. Chateau, J. Favier, U. D'Ortona, and S. Poncet, J. Fluid Mech. **824**, 931 (2017).
[17] E. Knight-Jones, J. Cell Sci. **s3-95**, 503 (1954).
[18] H. Machemer, J. Exp. Biol. **57**, 239 (1972).
[19] M. J. Sanderson and M. A. Sleigh, J. Cell Sci. **47**, 331 (1981).
[20] L. Wong, I. F. Miller, and D. B. Yeates, J. Appl. Physiol. **75**, 458 (1993).
[21] M. Ryser, A. Burn, T. Wessel, M. Frenz, and J. Rička, Eur. Biophys. J. **37**, 35 (2007).
[22] E. K. Vladar, J. V. Nayak, C. E. Milla, and J. D. Axelrod, JCI Insight **1**, 13 (2016).
[23] See Supplemental Material at http://link.aps.org/supplemental/10.1103/PhysRevLett.129.038101, which includes Refs. [24–31] for details about simulation methods.
[24] Y. Ding, J. C. Nawroth, M. J. McFall-Ngai, and E. Kanso, J. Fluid Mech. **743**, 124 (2014).
[25] H. Guo, L. Fauci, M. Shelley, and E. Kanso, J. Fluid Mech. **836**, 304 (2018).
[26] Z. Chai, B. Shi, Z. Guo, and F. Rong, J. Non-Newtonian Fluid Mech. **166**, 332 (2011).
[27] J. F. Doyle, *Nonlinear Analysis of Thin-Walled Structures: Statics, Dynamics, and Stability* (Springer Science & Business Media, Berlin, 2001).
[28] S. Gsell, U. D'Ortona, and J. Favier, Phys. Rev. E **100**, 033306 (2019).
[29] Z. Li, J. Favier, U. D'Ortona, and S. Poncet, J. Comput. Phys. **304**, 424 (2016).

[30] C. Wang and H. Tang, Bioinspiration Biomimetics **14**, 016011 (2018).
[31] C. Wang and H. Tang, J. Fluids Struct. **86**, 170 (2019).
[32] B. Button, L.-H. Cai, C. Ehre, M. Kesimer, D. B. Hill, J. K. Sheehan, R. C. Boucher, and M. Rubinstein, Science **337**, 937 (2012).
[33] J. Favier, A. Revell, and A. Pinelli, J. Comput. Phys. **261**, 145 (2014).
[34] D. B. Hill, V. Swaminathan, A. Estes, J. Cribb, E. T. O'Brien, C. W. Davis, and R. Superfine, Biophys. J. **98**, 57 (2010).
[35] B. Guirao, A. Meunier, S. Mortaud, A. Aguilar, J.-M. Corsi, L. Strehl, Y. Hirota, A. Desoeuvre, C. Boutin, Y.-G. Han *et al.*, Nat. Cell Biol. **12**, 341 (2010).
[36] S. Gsell, E. Loiseau, U. D'Ortona, A. Viallat, and J. Favier, Sci. Rep. **10**, 8405 (2020).